THE JOURNAL OF PHYSICAL CHEMISTRY C

Article

pubs.acs.org/JPCC

Probing the Structures of Neutral B_{11} and B_{12} Using High-Resolution Photoelectron Imaging of B_{11}^- and B_{12}^-

Joseph Czekner, Ling Fung Cheung, and Lai-Sheng Wang*

Department of Chemistry, Brown University, 324 Brook Street, Providence, Rhode Island 02912, United States

Supporting Information

ABSTRACT: We report high-resolution photoelectron imaging of B_{11}^- and B_{12}^- at 354.7 and 532.0 nm, respectively, resolving several low-frequency vibrational modes for neutral B_{11} and B_{12}. The vibrational information is highly valuable to verify the structures of the neutral clusters. Several isomers are considered, and vibrational frequencies are calculated for B_{11} and B_{12} using density functional theory. Comparisons between the experimental and calculated vibrational frequencies prove that the B_{11} neutral and anion both possess a perfectly planar C_{2v} structure. The B_{12}^- anion is quasi-planar with C_s symmetry, while the experiment confirms that neutral B_{12} possesses C_{3v} symmetry. The high-resolution photoelectron spectra also allow the electron affinities of B_{11} and B_{12} to be measured more accurately as 3.401 ± 0.002 and 2.221 ± 0.002 eV, respectively. It is shown that high-resolution photoelectron imaging can be an effective method to determine structures of small neutral boron clusters, complementary to infrared spectroscopy.

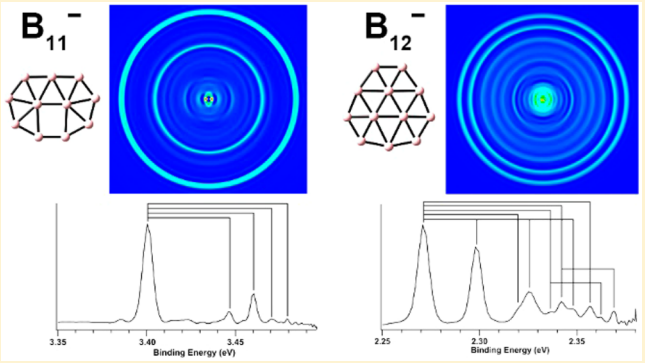

1. INTRODUCTION

The study of size-selected boron clusters has become an increasingly active area of research.[1−4] Before the year 2000, very few experimental studies existed on boron clusters. Anderson and coworkers first produced small cationic boron clusters using a laser vaporization source and tried to probe the stability of these clusters using collision-induced dissociation[5] as well as chemical reactions of the cationic clusters with small molecules.[6−9] These studies stimulated significant early theoretical calculations on small boron clusters.[10−19] However, there was no experimental information about the structures of boron clusters until 2002,[20−22] when photoelectron spectroscopy (PES) of size-selected negatively charged boron clusters was combined with global minimum searches and computational chemistry to probe the structures and chemical bonding of boron clusters, whereas in 2007 ion mobility was applied to probe the structures of size-selected cationic boron clusters up to B_{25}^+.[3] In contrast with bulk boron, where 3D cages are prevalent, small boron clusters are found to possess 2D structures.[23−34]

The chemical bonding of the 2D boron clusters is interesting. While the B−B bonds on the periphery of the 2D boron clusters can be described by classical two-center two-electron (2c−2e) bonds, the bonding among the interior boron atoms is characterized by delocalized multicenter bonding, giving rise to concepts of σ and π aromaticity/antiaromaticity and analogies to polycyclic aromatic hydrocarbons.[1,35] Even though the ion-mobility experiment suggested that 3D structures were already competitive at B_{16}^+ for cationic clusters,[3] low-lying 3D structures only appeared in B_{28}^- for anionic clusters.[36] Planar structures are still pervasive at larger clusters,[37,38] culminated with the discovery of the 2D B_{36}^-/B_{36} and B_{35}^- clusters, which feature hexagonal holes and provide indirect experimental evidence of the viability of atomically thin 2D borons, dubbed borospheres.[39,40] The recent successful syntheses of borophenes on inert substrate have stimulated significant further interests into this new class of 2D materials.[41,42] Another exciting development has been the discovery of the first all-boron cage cluster at B_{40} (borospherene).[43] Further studies suggest that there may be a class of borospherenes.[44,45]

The new experimental findings have stimulated significant theoretical interests.[46−64] While most calculations focus on neutral boron clusters, experimental studies on neutral boron clusters are extremely challenging. For example, the theoretical prediction of the interesting tubular B_{20} cluster still has not been confirmed experimentally.[1,26] The first experiment on neutral boron clusters has been an infrared/ultraviolet (IR/UV) two-color experiment on B_{11}, B_{16}, and B_{17} neutral clusters,[65] yielding vibrational information for these clusters between 650 and 1550 cm^{-1}. Vibrational frequencies provide an important piece of information for structural identification. Previously, only limited vibrational information was available from PES experiments of size-selected boron cluster anions using the magnetic-bottle photoelectron analyzer. Here we report high-

Special Issue: ISSPIC XVIII: International Symposium on Small Particles and Inorganic Clusters 2016

Received: October 31, 2016
Revised: December 9, 2016
Published: December 12, 2016

DOI: 10.1021/acs.jpcc.6b10958
J. Phys. Chem. C 2017, 121, 10752−10759

resolution photoelectron imaging of B_{11}^- and B_{12}^-, allowing low-frequency modes to be resolved for B_{11} and B_{12}.

High-resolution photoelectron imaging has become a powerful technique to yield vibrational information for structure determinations of both anionic and neutral clusters.[66−68] The current experiments provide strong evidence that the B_{11} neutral and anion clusters possess a perfectly planar C_{2v} structure. We further confirm that the B_{12}^- anion is a quasi-planar bowl-shaped cluster with C_s symmetry, but the neutral B_{12} possesses a C_{3v} structure. In addition, the high-resolution PES data allow the electron affinities (EAs) of B_{11} and B_{12} to be measured more accurately as 3.401 ± 0.002 and 2.221 ± 0.002 eV, respectively. The current study suggests that high-resolution PE imaging can be combined with computational chemistry to study not only the structures and bonding of anionic clusters, but also the structures of the corresponding neutral species.

2. EXPERIMENTAL AND COMPUTATIONAL METHODS

2.1. Experimental Method. The experiments were performed using a laser vaporization supersonic cluster source coupled to a high-resolution velocity-map imaging (VMI) detector, details of which can be found elsewhere.[69−71] In brief, boron clusters were produced from a disk target compressed from a mixture of bismuth and isotopically enriched ^{11}B powder (5:1 ratio by mass). The bismuth acted as a binder and provided a convenient source of Bi^- for calibration. The second harmonic of a 10 Hz Nd:YAG laser was used as the vaporization laser. A helium carrier gas seeded with 10% argon was pulsed into the nozzle to cool the laser-induced plasma to initiate nucleation. The clusters formed inside the nozzle were entrained in the carrier gas and underwent a supersonic expansion to produce a cold cluster beam. As previously shown, a longer residence time in the waiting room of the nozzle was crucial for producing vibrationally cold clusters.[1,72−74] After passing a skimmer, negatively charged boron clusters were extracted perpendicularly into a modified Wiley−McLaren time-of-flight mass spectrometer.

The B_{11}^- and B_{12}^- clusters of current interest were each mass-selected by a mass-gate before entering the interaction zone of the VMI lens assembly, where they were detached by a second Nd:YAG laser. The nascent photoelectrons were extracted and focused onto a phosphor screen coupled to a set of microchannel plates and a charged-coupled device camera. A high-quality Glan-laser polarizer ensured that the detachment laser polarization was parallel with the imaging detector. Each experiment for B_{11}^- and B_{12}^- required about 200 000 shots to achieve satisfactory signal-to-noise ratios. The VMI lens system was calibrated using the known detachment transitions of Au^- and Bi^-. Our typical kinetic energy resolution ($\Delta E_k/E_k$) is ~0.6% for high kinetic energy electrons and as low as 1.2 cm^{-1} (fwhm) for low kinetic energy electrons.[70] The raw images were analyzed using the Maximum Entropy Velocity Legendre Reconstruction program (MEVELER).[75] We also compared the MEVELER results to those using both the BASEX[76] and pBASEX[77] methods, which yielded similar spectra.

2.2. Photoelectron Angular Distributions. Another piece of information obtained from photoelectron imaging is the electron angular distributions, characterized by the anisotropy parameter (β). The differential cross section of the photoelectrons is described by

$$d\sigma/d\Omega = (\sigma_{tot}/4\pi)[1 + \beta P_2(\cos\theta)] \quad (1)$$

where σ_{tot} is the total differential cross-section, P_2 is the second-order Legendre polynomial, and θ is the angle of the detached electron relative to the laser polarization.[78] Hence, the photoelectron angular distribution (PAD) is described by

$$dI(\theta) \approx [1 + \beta P_2(\cos\theta)] \quad (2)$$

where β is the anisotropy parameter, which has values between −1 and 2. This model works well for single photon transitions from randomly oriented particles. Because photons carry one unit of angular momentum ($l = \pm 1$), the outgoing photoelectron wave will have an identical change in their angular momentum upon detachment. For example, when an electron is detached from an s orbital ($l = 0$), the ejected electron will have $l = 1$ (pure p-wave) with $\beta = 2$. Interpreting the β value for a molecular orbital is not a trivial process[79] due to the fact that molecular orbitals are approximated as linear combinations of atomic orbitals. Nevertheless, the values of β can be used to qualitatively assess the molecular orbital shape.

2.3. Theoretical Method. Previously reported structures for B_{11}^- and B_{12}^- were reoptimized using the B3LYP hybrid functional[80,81] with the Def2-TZVPPD basis set[82−84] in the Gaussian 09 program suite.[85] Harmonic vibrational frequencies were calculated to ensure that the structures were minima on the potential energy surfaces. We used the optimized anion structures as the starting point for the geometry optimization and frequency calculations of the neutral clusters. The optimized anion structures were used for single-point energy calculations for the neutral clusters to compute the vertical detachment energies (VDEs). The calculated vibrational frequencies for the neutral clusters are used to compare with the experimental data without any scaling.

3. RESULTS

3.1. High-Resolution PE Imaging of B_{11}^-. The high-resolution PE image and spectrum of B_{11}^- at 354.7 nm (3.496 eV) are shown in Figure 1, which is relatively simple. There is

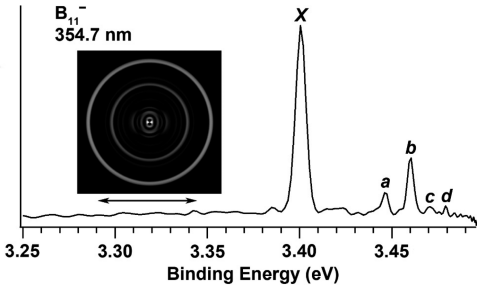

Figure 1. Photoelectron image and spectrum of B_{11}^- at 354.7 nm (3.496 eV). The resolved vibrational features are labeled. The peak *X* represents the 0−0 detachment transition and defines the adiabatic and vertical detachment energies of B_{11}^-. The horizontal arrows below the image denote the laser polarization.

an intense peak labeled *X* at 3.401 ± 0.002 eV, which represents the detachment transition from the ground vibrational level of B_{11}^- to the ground vibrational level of the ground electronic state of B_{11} (the 0−0 transition). The *X* peak defines the adiabatic detachment energy (ADE) or EA of B_{11}. The fact that the 0−0 transition is the most intense peak suggests that there are very small geometry changes between the anion and the neutral final state. In this case, the ADE and VDE become

DOI: 10.1021/acs.jpcc.6b10958
J. Phys. Chem. C 2017, 121, 10752−10759

Table 1. Summary of First Experimental Vertical Detachment Energy (VDE) for B_{11}^- and B_{12}^- and Vibrational Frequencies Observed for B_{11} and B_{12} Compared with Theoretical Calculations[a]

B_{11}^-/B_{11}									
experimental				theoretical					
peak	VDE (eV)[b]	peak	frequencies (cm^{-1})[c]	VDEs (eV)			frequencies (cm^{-1})		
				11-I	11-II	11-IV	11-V	11-VI	11-VII
X	3.401(2)	*a*	380	3.38	3.25	2.81	374	246	311
	[0.07]	*b*	490				491	348	529
		c	560				564	413	610
		d	640				634	446	613
			1040[d]				1017	1101	1022
B_{12}^-/B_{12}									
experimental				theoretical					
peak	VDE (eV)[b]	peak	frequencies (cm^{-1})[c]	VDEs (eV)			frequencies (cm^{-1})		
				12-I	12-II		12-IV	12-V	
X	2.221(2)	*a*	220	2.22	2.48		227		
	[0.17]	*b*	390*				405	467	
							454		
							474		
							514		
		c	540*				545		
		d	580				582	605	
		e	690				686	729	

[a]Only allowed transitions are displayed for the calculated frequencies. Complete sets of calculated frequencies are presented in the Supporting Information. [b]Value in parentheses represents the experimental uncertainty and the value in brackets is the anisotropy parameter (β) from fitting eq 2 to peak X. [c]All measured frequencies have an uncertainty of ±20 cm^{-1} unless denoted with "*", which have an estimated uncertainty of ±50 cm^{-1} due to the fact the peaks are not fully resolved. [d]This mode was observed in a previous report[24] and could not be measured in the current experiment due to the low photon energy.

the same value experimentally because the VDE is measured as the strongest vibrational peak in a vibronic transition. Four weaker peaks, *a*, *b*, *c*, and *d*, are observed at slightly higher binding energies, and they should represent vibrationally excited levels of the B_{11} ground electronic state. The separations of these peaks from peak *X* are listed in Table 1 as the experimental vibrational frequencies. There is a very weak peak present around 3.385 eV, which appeared only when the MEVELER program was used. Hence, it was likely an artifact of the data inversion method. Only the intense 0−0 peak *X* could be accurately fit by eq 2 to obtain a value for β, which was found to be 0.07.

The previously reported low-resolution PE spectrum of B_{11}^- at 266 nm showed that the ground-state detachment transition consisted of a long vibrational progression up to ~3.8 eV binding energy.[24] Two vibrational frequencies were obtained: a high frequency at 1040 ± 50 cm^{-1} and a low frequency at 480 ± 40 cm^{-1}. The current high-resolution spectrum at 354.7 nm only represents the threshold region of the ground-state detachment transition of B_{11}^-. The 490 cm^{-1} vibrational frequency (peak *b*) should correspond to the lower frequency (480 ± 40 cm^{-1}) observed previously. In addition to the three additional vibrational modes (*a*, *c*, and *d*) and the more accurate vibrational frequencies, the EA for B_{11} obtained in the current study is also much more accurate than that observed previously (3.426 ± 0.010 eV). In fact, the 0.010 eV uncertainty given previously appeared to be too small.[24]

3.2. High-Resolution PE Imaging of B_{12}^-. The high-resolution PE image and spectrum of B_{12}^- are shown in Figure 2 at 532.0 nm (2.331 eV). The high-resolution spectrum for B_{12}^- is slightly more complicated, with many more vibrational features. Again, the peak labeled as *X*, at 2.221 ± 0.002 eV,

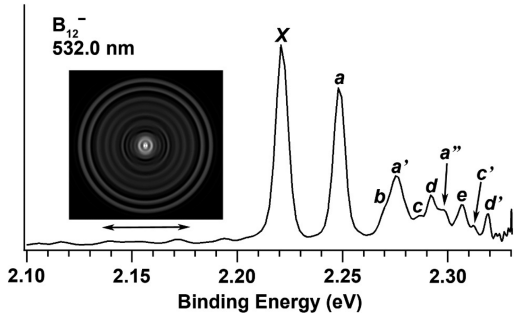

Figure 2. Photoelectron image and spectrum of B_{12}^- at 532.0 nm (2.331 eV). The resolved vibrational features are labeled. The peak *X* represents the 0−0 detachment transition and defines the adiabatic and vertical detachment energies of B_{11}^-. The horizontal arrows below the image denote the laser polarization.

denotes the 0−0 transition, representing the ADE and VDE or the EA of B_{12}. A vibrational progression with a frequency of 220 ± 20 cm^{-1} can be identified up to the third quanta, labeled as *a*, *a*′, and *a*″, which should correspond to the most Franck−Condon-active vibrational mode. The peak *a*′ at 2.276 eV has a small shoulder on the left side (labeled as *b*). We deconvoluted this peak with two Gaussian functions to locate the peak position of *b* at 2.269 eV, which should correspond to a different vibrational mode. There appears to be a weak peak at 2.287 eV (*c*), with a separation from peak *X* at 540 ± 50 cm^{-1}, which should represent a new vibrational mode. There is a peak ~220 cm^{-1} higher in energy than peak *c*, denoted as *c*′. Peak *d* is found to be 580 ± 20 cm^{-1} higher in energy than peak *X*. There is also a well-resolved peak (*d*′), that has the same separation of 220 cm^{-1}, in agreement with progression *a*. These

DOI: 10.1021/acs.jpcc.6b10958
J. Phys. Chem. C 2017, 121, 10752−10759

peaks should correspond to combination levels with the most Franck−Condon-active mode. Finally, peak *e*, which is 690 ± 20 cm^{-1} above peak *X*, is also observed and should correspond to a higher frequency mode. The peaks *X* and *a* both had sufficient signal-to-noise ratios to allow good fits with eq 2. The β values determined are 0.17 for both peaks.

The previous PES study of B_{12}^- at different photon energies revealed a large energy gap (2.0 eV),[24] suggesting that the neutral B_{12} is an extremely stable electronic system. The ground-state detachment transition was an almost feature-less broad band (extending to ~2.7 eV), suggesting a relatively large geometry change between B_{12}^- and B_{12}. Hence the current high-resolution spectrum at 532.0 nm only represents part of the Franck−Condon region of the ground-state detachment transition of B_{12}^-. The current EA of 2.221 ± 0.002 eV is much more accurate than the previous value of 2.21 ± 0.04 eV.[24] It should be pointed out that no discernible vibrational hot bands were observed in either of the B_{11}^- and B_{12}^- spectra (Figures 1 and 2), suggesting the effectiveness of vibrational cooling in our supersonic cluster source.[1,72−74]

3.3. Computational Results. We performed theoretical calculations to understand the observed vibrational structures for B_{11} and B_{12} and to assist the spectral assignments. We used the previously reported anion structures at the PW91 level of theory[24] as starting points for the current calculations. The relative energies of the reoptimized anion structures at the B3LYP level of theory are shown in Figure 3. For B_{11}^-, the perfectly planar C_{2v} structure (isomer 11-I, $^1A_1$) is the lowest energy structure, same as before. The ordering of the three high-energy isomers is also similar, except the relative energies changed slightly. For example, the quasi-planar isomer 11-II is 1.20 eV higher in energy than the global minimum in the current calculation, but it was 0.84 eV higher in the previous calculation. For B_{12}^-, only three of the five previously reported isomers were found to be minima at the current level of theory. The global minimum is a slightly distorted quasi-planar bowl-shaped structure with C_s symmetry (12-I, $^2A'$). The next isomer (12-II, ^2A_u) is a planar structure with C_{2h} symmetry, which is 0.96 eV higher in energy relative to the global minimum. A 3D structure lies 1.90 eV higher in energy (12-III, D_{2h}). The energy ordering of the two higher-lying isomers 12-II and 12-III is reversed compared with the previous study.[24]

For B_{11}, we found isomer 11-V ($^2B_2$) is the lowest in energy with the similar planar C_{2v} structure as the anion. Isomers 11-VI and 11-VII are 1.12 and 2.90 eV higher in energy. The optimization of the neutral structure corresponding to isomer 11-III of the anion yielded an imaginary frequency. The global minima for the B_{11} anion and neutral in the current calculations are the same as reported previously,[24] which have also been confirmed by other previous studies.[55,65] The calculated first VDEs for isomers 11-I, 11-II, and 11-IV of B_{11}^- are presented in Table 1, along with the four lowest totally symmetric vibrational frequencies of the neutral isomers. Figure 4A displays the displacement vectors of several totally symmetric vibrational modes for isomer 11-V observed in the PES experiments. We did not present a calculated VDE or vibrational frequencies for isomer 11-III because the neutral isomer is not a minimum. The calculated vibrational

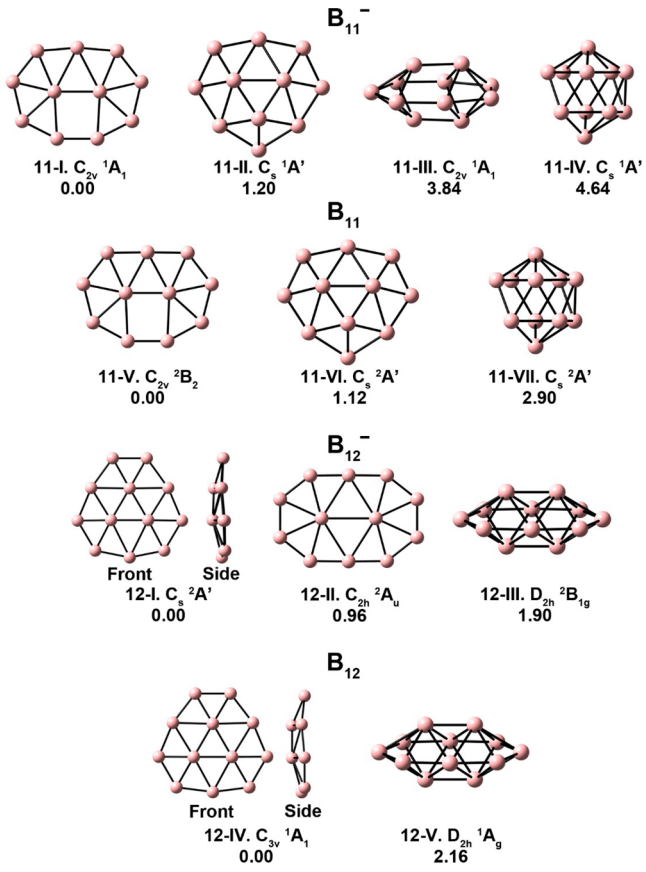

Figure 3. Optimized structures for B_{11} and B_{12} anion and neutral clusters. The zero-point-corrected energies relative to the global minima are given in electronvolts. The calculations were done using the B3LYP method with the Def2-TZVPPD basis set.

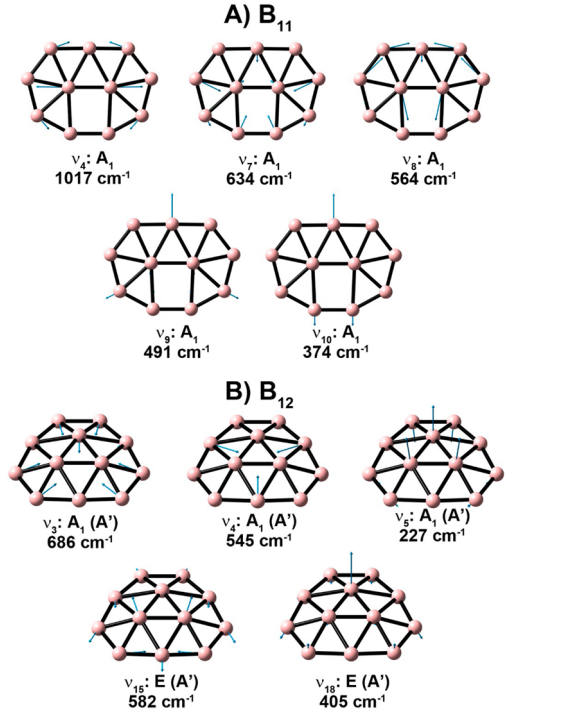

Figure 4. Displacement vectors for the observed vibrational modes with the calculated frequencies of (A) isomer 11-V of B_{11} and (B) isomer 12-IV of B_{12}. The symmetry is shown for the neutral structures along with the reduced symmetry for the C_s anion for B_{12}^- in parentheses.

DOI: 10.1021/acs.jpcc.6b10958
J. Phys. Chem. C 2017, 121, 10752−10759

frequencies for all the vibrational modes for the three neutral isomers are given in the Supporting Information (Table S1).

For neutral B_{12}, only isomers 12-I and 12-III yielded neutral structures that did not contain any imaginary frequencies. Isomer 12-I optimized to a C_{3v} structure in the neutral labeled as 12-IV. The 3D isomer 12-V is much higher in energy than the global minimum, which means both the anion and neutral should possess a quasi-planar structure. The C_{3v} B_{12} structure in the current study is in accord with previous calculations.[15,24,55] The calculated first VDEs for isomers 12-I and 12-III are given in Table 1 with the symmetry-allowed modes of isomers 12-IV and 12-V, in comparison with the experimental data. Figure 4B exhibits the vibrational displacement vectors for several modes of isomer 12-IV, which are observed experimentally (vide infra).

4. DISCUSSION

4.1. Structures of B_{11}^- and B_{11} and the Vibrational Assignments. The previous PES study using a magnetic-bottle analyzer[24] revealed two vibrational frequencies at 1040 ± 50 and 480 ± 40 cm^{-1}. The higher frequency mode was in good agreement with the calculated frequency for the B−B stretching mode (1,017 cm^{-1}) of the inner boron atoms of isomer 11-V (ν_4 in Figure 4A), as also previously explained.[24] The smaller vibrational frequency matched the calculated frequency of mode ν_9 in Table 1 and Figure 4A, where three peripheral boron atoms are symmetrically stretching with respect to the two center atoms. The previous IR/UV two-color experiments on neutral B_{11} revealed an intense peak near 915 cm^{-1} and a weaker peak around 1220 cm^{-1}.[65] These two frequencies agree well with the IR-active modes, ν_{22} (B_2) and ν_{20} (B_2), with computed frequencies at 979 and 1267 cm^{-1}, respectively (Table S1). The simulated IR spectrum for isomer 11-V was in good agreement with the experimental data, providing considerable credence that the global minimum of B_{11} is the C_{2v} structure in Figure 3. The current high-resolution PE imaging data allowed us to resolve several more low vibrational frequency modes not observed previously.

The current PE spectrum for B_{11}^- is relatively simple for two reasons. First, the photon energy of the detachment laser was too low and only the threshold region of the ground-state detachment transition was accessible. Second, the limited number of peaks indicates a relatively symmetric structure for the anion and neutral. In addition, the low intensities for the vibrationally excited states suggest the structural change upon electron detachment is small, giving rise to the same value for the ADE and VDE, as defined by peak *X* at 3.401 ± 0.002 eV in Figure 1. The observed VDE is in good agreement with the calculated first VDE (3.38 eV) for the global minimum 11-I, as shown in Table 1. Isomers 11-II and 11-IV can be clearly ruled out on the basis of their first calculated VDEs as well as the calculated vibrational frequencies to be discussed below.

Peak *b* is the most intense excited vibrational peak, yielding a frequency of 490 ± 20 cm^{-1}. This vibrational peak should be the same as the 480 ± 40 cm^{-1} vibrational frequency observed previously,[24] corresponding to the ν_9 mode (Figure 4A). Three new vibrational frequencies are resolved in the current experiment, which have much lower intensities. The lowest frequency observed is 380 ± 20 cm^{-1}, corresponding to peak *a*. This frequency is in very good agreement with the ν_{10} mode with a calculated frequency of 374 cm^{-1} (Table 1 and Figure 4A). The peaks *c* and *d* give rise to two higher vibrational frequencies at 560 and 640 cm^{-1}, respectively, which can be readily assigned to the ν_8 and ν_7 modes with calculated frequencies at 564 and 640 cm^{-1} (Table 1 and Figure 4A). All four modes observed are in-plane vibrational modes with A_1 symmetry, consistent with the fact that both the B_{11} anion and the neutral have the same C_{2v} symmetry and only totally symmetric modes are allowed.

Figure 5 shows the highest occupied molecular orbital (HOMO) of B_{11}^-, from which the electron is detached. This orbital involves complicated delocalized σ-bonding over the entire cluster plane, consistent with the observed vibrational structures and the minor geometry changes between the anion and the neutral. The HOMO has B_2 symmetry and can be viewed as involving in-plane p orbitals of the peripheral boron atoms. On the basis of the s&p model,[79] detachment from a molecular orbital with B_2 symmetry should produce a combination of isotropic (s-wave) and perpendicular (s+d-wave) partial waves. We observe a nearly isotropic distribution ($\beta = 0.07$), which is consistent with this prediction and suggests the isotropic wave dominates at low electron kinetic energies.

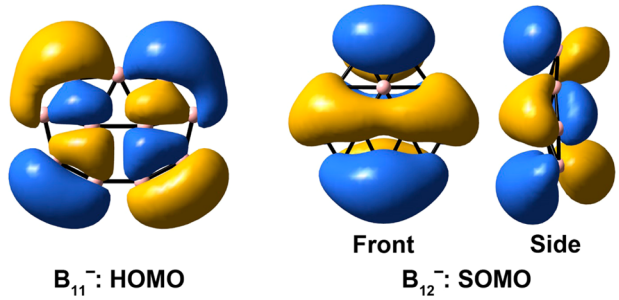

Figure 5. Molecular orbital pictures for the highest occupied molecular orbital (HOMO) of B_{11}^- (C_{2v}, $^1A_1$) and the singly occupied molecular orbital (SOMO) of B_{12}^- (C_s, $^2A'$).

4.2. Vibrational Assignment and the Structures of B_{12}^- and B_{12}. An ADE and VDE of 2.21 ± 0.04 and 2.26 ± 0.04 eV were reported for B_{12}^-, respectively, in the previous PES study.[24] The difference in the ADE and VDE was due to the low spectral resolution and broad PES features. The current high-resolution spectrum suggests that the ADE and VDE are the same, as defined by the X peak (Figure 2), suggesting that the structural change between the anion and the neutral is not too great. The more accurate VDE of 2.221 eV from the current experiment is in excellent agreement with the computed VDE (2.22 eV) for the global minimum 12-I isomer of B_{12}^- with C_s symmetry ($^2A'$), consistent with the previous study.[24] The current calculations also agree with the previous report that the B_{12}^- anion is a doublet with a singly occupied molecular orbital (SOMO), as shown in Figure 5. The SOMO is a delocalized π orbital with both bonding and antibonding characters in different parts of the bowl-shaped cluster.

Numerous vibrational peaks are resolved at higher binding energies in the current experiment on B_{12}^-, as shown in Figure 2. The congested vibrational features are consistent with the fact that there is a change of symmetry from C_s to C_{3v} between the anion and the neutral, resulting in many more allowed vibrational modes in the PE spectrum. There is a relatively extended vibrational progression of 220 cm^{-1} consisting of peaks *a*, *a'*, and *a''*, in excellent agreement with mode ν_5 with a calculated frequency of 227 cm^{-1} (Table 1). This is the most Franck−Condon active mode, corresponding primarily to the out-of-plane motion of the three center atoms that distort the

DOI: 10.1021/acs.jpcc.6b10958
J. Phys. Chem. C 2017, 121, 10752−10759

C_{3v} symmetry of the neutral to C_s in the anion (Figure 4B). Peak *b*, ~390 ± 50 cm^{-1} above peak *X*, should correspond to mode ν_{18} with a calculated frequency of 405 cm^{-1}, involving mainly the out-of-plane motion of one of the center atom (Figure 4B). Peak *c* at 540 cm^{-1} is in good agreement with the calculated frequency of the ν_4 mode (545 cm^{-1}), which involves the symmetric stretching of three peripheral boron atoms (Figure 4b). The small weak *c′* about 220 cm^{-1} above peak *c* is attributed to a combinational level of modes ν_4 and ν_5. Peak *d* at 580 ± 20 cm^{-1} agrees with the calculated frequency of mode ν_{15} (582 cm^{-1}), involving mainly out-of-plane motion of two of the three central boron atoms. A combinational level between the ν_{15} and ν_5 modes is also observed, as indicated by peak *d′*, which is 220 cm^{-1} above peak *d*. Finally, peak *e* yields a frequency of 680 ± 20 cm^{-1}, which is in perfect agreement with the ν_3 totally symmetric breathing mode with a theoretical frequency of 686 cm^{-1}.

Removing an electron from the B_{12}^- SOMO (Figure 5) is expected to have a significant effect on the bowl shape of the quasi-planar cluster because of its bonding and antibonding characters in different parts of the cluster. The β value is not easy to interpret for electron detachment from this orbital, which is mainly comprised of p_z orbitals, consistent with the nearly isotropic distribution (β = 0.17). The shape of the SOMO can be used to understand the structural change between the anion and the neutral and the observed vibrational modes. The most active mode is the ν_5 mode (Figure 4B), which is consistent with the large change in planarity between the neutral and the anion. In particular, because the symmetry is lower in the anion, it is possible to observe vibrational modes with E symmetry of the neutral, which contains A′ irreducible representations under C_s symmetry (Table S2). The observation of the ν_{15} and ν_{18} modes with *E* symmetry proves that the B_{12}^- anion is a quasi-planar C_s structure. The excellent agreement between the observed and computed vibrational frequencies for the C_{3v} B_{12} structure provides additional evidence of the global minima of the B_{12} neutral and anionic cluster.

5. CONCLUSIONS

We report a high-resolution photoelectron imaging study of B_{11}^- and B_{12}^- with vibrational resolution. In addition to more accurate measurements of electron affinities for B_{11} (3.401 ± 0.002 eV) and B_{12} (2.221 ± 0.002 eV), we resolved several low-frequency vibrational modes less than 700 cm^{-1} for B_{11} and B_{12} for the first time. The observed vibrational structures are compared with theoretical calculations, providing firm confirmations for the C_{2v} structure for B_{11} and the C_{3v} structure for B_{12}. Combining the computed first VDEs and the symmetries of the observed vibrational modes also provides information for the global minima of the anions. Only totally symmetric modes are observed in the spectrum of B_{11}^- because both the anion and the neutral have the same symmetry. The observation of vibrational modes with *E* symmetry in the spectrum of B_{12}^- indicates that the anion has a lower symmetry (C_s). Photodetachment of an anion probes the potential energy surface of the corresponding neutral near that of the anion. The current study suggests that high-resolution photoelectron imaging of anion, in combination with careful global minimum searches, provides a complementary technique to provide vibrational and structural information for neutral boron clusters.

■ ASSOCIATED CONTENT

Supporting Information

The Supporting Information is available free of charge on the ACS Publications website at DOI: 10.1021/acs.jpcc.6b10958.

Calculated vibrational frequencies of all vibrational modes for the global minimum and two isomers of B_{11} and the global minimum and one low-lying isomer of B_{12} and full citations of references 36, 41, 43−45, and 85. (PDF)

■ AUTHOR INFORMATION

Corresponding Author

*E-mail: Lai-Sheng_Wang@brown.edu.

ORCID

Lai-Sheng Wang: 0000-0003-1816-5738

Notes

The authors declare no competing financial interest.

■ ACKNOWLEDGMENTS

This work was supported by the National Science Foundation under grant number CHE-1632813. Computational support was provided by Brown University's Center for Computation and Visualization.

■ REFERENCES

(1) Wang, L. S. Photoelectron Spectroscopy of Size-Selected Boron Clusters: From Planar Structures to Borophenes and Borospherenes. *Int. Rev. Phys. Chem.* **2016**, *35*, 69−142.

(2) Sergeeva, A. P.; Popov, I. A.; Piazza, Z. A.; Li, W. L.; Romanescu, C.; Wang, L. S.; Boldyrev, A. I. Understanding Boron through Size-Selected Clusters: Structure, Chemical Bonding, and Fluxionality. *Acc. Chem. Res.* **2014**, *47*, 1349−1358.

(3) Oger, E.; Crawford, N. R. M.; Kelting, R.; Weis, P.; Kappes, M. M.; Ahlrichs, R. Boron Cluster Cations: Transition from Planar to Cylindrical Structures. *Angew. Chem., Int. Ed.* **2007**, *46*, 8503−8506.

(4) Alexandrova, A. N.; Boldyrev, A. I.; Zhai, H. J.; Wang, L. S. All-Boron Aromatic Clusters as Potential New Inorganic Ligands and Building Blocks in Chemistry. *Coord. Chem. Rev.* **2006**, *250*, 2811−2866.

(5) Hanley, L.; Whitten, J. L.; Anderson, S. L. Collision-Induced Dissociation and ab Initio Studies of Boron Cluster Ions: Determination of Structures and Stabilities. *J. Phys. Chem.* **1988**, *92*, 5803−5812.

(6) Hanley, L.; Anderson, S. L. Oxidation of Small Boron Cluster Ions (B^+_{1-13}) by Oxygen. *J. Chem. Phys.* **1988**, *89*, 2848−2860.

(7) Hintz, P. A.; Ruatta, S. A.; Anderson, S. L. Interaction of Boron Cluster Ions with Water: Single Collision Dynamics and Sequential Etching. *J. Chem. Phys.* **1990**, *92*, 292−303.

(8) Hintz, P. A.; Sowa, M. B.; Ruatta, S. A.; Anderson, S. L. Reactions of Boron Clusters Ions (B^+_n, *n* = 2−24) with N_2O: NO versus NN Bond Activation as a Function of Size. *J. Chem. Phys.* **1991**, *94*, 6446−6458.

(9) Sowa-Resat, M. B.; Smolanoff, J.; Lapicki, A.; Anderson, S. L. Interaction of Small Boron Cluster Ions with HF. *J. Chem. Phys.* **1997**, *106*, 9511−9522.

(10) Kawai, R.; Weare, J. H. Instability of the B_{12} Icosahedral Cluster: Rearrangement to a Lower Energy Structure. *J. Chem. Phys.* **1991**, *95*, 1151−1159.

(11) Kawai, R.; Weare, J. H. Anomalous Stability of B^+_{13} Clusters. *Chem. Phys. Lett.* **1992**, *191*, 311−314.

(12) Bonačič-Koutecký, V.; Fantucci, P.; Koutecký, J. Quantum Chemistry of Small Clusters of Elements of Groups Ia, Ib, and IIa: Fundamental Concepts, Predictions, and Interpretation of Experiments. *Chem. Rev.* **1991**, *91*, 1035−1108.

DOI: 10.1021/acs.jpcc.6b10958
J. Phys. Chem. C 2017, 121, 10752−10759

(13) Kato, H.; Yamashita, K.; Morokuma, K. Ab initio MO Study of Neutral and Cationic Boron Clusters. *Chem. Phys. Lett.* **1992**, *190*, 361−366.
(14) Boustani, I. Structure and Stability of Small Boron Clusters. A Density Functional Theoretical Study. *Chem. Phys. Lett.* **1995**, *240*, 135−140.
(15) Boustani, I. Systematic ab Initio Investigation of Bare Boron Clusters: Determination of the Geometry and Electronic Structures of B_n (n = 2−14). *Phys. Rev. B: Condens. Matter Mater. Phys.* **1997**, *55*, 16426−16438.
(16) Ricca, A.; Bauschlicher, C. W., Jr. The Structure and Stability of B^+_n Clusters. *Chem. Phys.* **1996**, *208*, 233−242.
(17) Gu, F. L.; Yang, X.; Tang, A. C.; Jiao, H.; Schleyer, P. V. R. Structure and Stability of B_{13}^+ Clusters. *J. Comput. Chem.* **1998**, *19*, 203−214.
(18) Fowler, J. E.; Ugalde, J. M. The Curiously Stable B_{13}^+ Cluster and its Neutral and Anionic Counterparts: The Advantages of Planarity. *J. Phys. Chem. A* **2000**, *104*, 397−403.
(19) Aihara, J. B_{13}^+ is Highly Aromatic. *J. Phys. Chem. A* **2001**, *105*, 5486−5489.
(20) Zhai, H. J.; Wang, L. S.; Alexandrova, A. N.; Boldyrev, A. I. On the Electronic Structure and Chemical Bonding of B_5^- and B_5 by Photoelectron Spectroscopy and ab Initio Calculations. *J. Chem. Phys.* **2002**, *117*, 7917−7924.
(21) Alexandrova, A. N.; Boldyrev, A. I.; Zhai, H. J.; Wang, L. S.; Steiner, E.; Fowler, P. W. Structure and Bonding in B_6^- and B_6: Planarity and Antiaromaticity. *J. Phys. Chem. A* **2003**, *107*, 1359−1369.
(22) Zhai, H. J.; Wang, L. S.; Alexandrova, A. N.; Boldyrev, A. I.; Zakrzewski, V. G. Photoelectron Spectroscopy and ab Initio Study of B_3^- and B_4^- Anions and Their Neutrals. *J. Phys. Chem. A* **2003**, *107*, 9319−9328.
(23) Zhai, H. J.; Alexandrova, A. N.; Birch, K. A.; Boldyrev, A. I.; Wang, L. S. Hepta- and Octa-Coordinated Boron in Molecular Wheels of Eight- and Nine-Atom Boron Clusters: Observation and Confirmation. *Angew. Chem., Int. Ed.* **2003**, *42*, 6004−6008.
(24) Zhai, H. J.; Kiran, B.; Li, J.; Wang, L. S. Hydrocarbon Analogs of Boron Clusters: Planarity, Aromaticity, and Antiaromaticity. *Nat. Mater.* **2003**, *2*, 827−833.
(25) Alexandrova, A. N.; Boldyrev, A. I.; Zhai, H. J.; Wang, L. S. Electronic Structure, Isomerism, and Chemical Bonding in B_7^- and B_7. *J. Phys. Chem. A* **2004**, *108*, 3509−3517.
(26) Kiran, B.; Bulusu, S.; Zhai, H. J.; Yoo, S.; Zeng, X. C.; Wang, L. S. Planar-to-Tubular Structural Transition in Boron Clusters: B_{20} as the Embryo of Single-Walled Boron Nanotubes. *Proc. Natl. Acad. Sci. U. S. A.* **2005**, *102*, 961−964.
(27) Sergeeva, A. P.; Zubarev, D. Y.; Zhai, H. J.; Boldyrev, A. I.; Wang, L. S. A Photoelectron Spectroscopic and Theoretical Study of B_{16}^- and B_{16}^{2-}: An All-Boron Naphthalene. *J. Am. Chem. Soc.* **2008**, *130*, 7244−7246.
(28) Huang, W.; Sergeeva, A. P.; Zhai, H. J.; Averkiev, B. B.; Wang, L. S.; Boldyrev, A. I. A Concentric Planar Doubly π-Aromatic B_{19}^- Cluster. *Nat. Chem.* **2010**, *2*, 202−206.
(29) Sergeeva, A. P.; Averkiev, B. B.; Zhai, H. J.; Boldyrev, A. I.; Wang, L. S. All-Boron Analogues of Aromatic Hydrocarbons: B_{17}^- and B_{18}^-. *J. Chem. Phys.* **2011**, *134*, 224304.
(30) Piazza, Z. A.; Li, W. L.; Romanescu, C.; Sergeeva, A. P.; Wang, L. S.; Boldyrev, A. I. A Photoelectron Spectroscopy and ab Initio Study of B_{21}^-: Negatively Charged Boron Clusters Continue to Be Planar at 21. *J. Chem. Phys.* **2012**, *136*, 104310.
(31) Sergeeva, A. P.; Piazza, Z. A.; Romanescu, C.; Li, W. L.; Boldyrev, A. I.; Wang, L. S. B_{22}^- and B_{23}^-: All-Boron Analogues of Anthracene and Phenanthrene. *J. Am. Chem. Soc.* **2012**, *134*, 18065−18073.
(32) Popov, I. A.; Piazza, Z. A.; Li, W. L.; Wang, L. S.; Boldyrev, A. I. A Combined Photoelectron Spectroscopy and ab Initio Study of the Quasi-Planar B_{24}^- Cluster. *J. Chem. Phys.* **2013**, *139*, 144307.
(33) Piazza, Z. A.; Popov, I. A.; Li, W. L.; Pal, R.; Zeng, X. C.; Boldyrev, A. I.; Wang, L. S. A Photoelectron Spectroscopic and ab Initio Study of the Structures and Chemical Bonding of the B_{25}^- Cluster. *J. Chem. Phys.* **2014**, *141*, 034303.
(34) Li, W. L.; Pal, R.; Piazza, Z. A.; Zeng, X. C.; Wang, L. S. B_{27}^-: Appearance of the Smallest Planar Boron Cluster Containing a Hexagonal Vacancy. *J. Chem. Phys.* **2015**, *142*, 204305.
(35) Boldyrev, A. I.; Wang, L. S. Beyond Organic Chemistry: Aromaticity in Atomic Clusters. *Phys. Chem. Chem. Phys.* **2016**, *18*, 11589−11605.
(36) Wang, Y. J.; Zhao, Y. F.; Li, W. L.; Jian, T.; Chen, Q.; You, X. R.; Ou, T.; Zhao, X. Y.; Zhai, H. J.; Li, S. D.; et al. Observation and Characterization of the Smallest Borospherene, B_{28}^- and B_{28}. *J. Chem. Phys.* **2016**, *144*, 064307.
(37) Li, H. R.; Jian, T.; Li, W. L.; Miao, C. Q.; Wang, Y. J.; Chen, Q.; Luo, X. M.; Wang, K.; Zhai, H. J.; Li, S. D.; Wang, L. S. Competition between Quasi-Planar and Cage-Like Structures in the B_{29}^- Cluster: Photoelectron Spectroscopy and *Ab Initio* Calculations. *Phys. Chem. Chem. Phys.* **2016**, *18*, 29147−29155.
(38) Li, W. L.; Zhao, Y. F.; Hu, H. S.; Li, J.; Wang, L. S. B_{30}^-: A Quasiplanar Chiral Boron Cluster. *Angew. Chem., Int. Ed.* **2014**, *53*, 5540−5545.
(39) Piazza, Z. A.; Hu, H. S.; Li, W. L.; Zhao, Y. F.; Li, J.; Wang, L. S. Planar Hexagonal B_{36} as a Potential Basis for Extended Single-Atom Layer Boron Sheets. *Nat. Commun.* **2014**, *5*, 3113.
(40) Li, W. L.; Chen, Q.; Tian, W. J.; Bai, H.; Zhao, Y. F.; Hu, H. S.; Li, J.; Zhai, H. J.; Li, S. D.; Wang, L. S. The B_{35} Cluster with a Double-Hexagonal Vacancy: A New and More Flexible Structural Motif for Borophene. *J. Am. Chem. Soc.* **2014**, *136*, 12257−12260.
(41) Mannix, A. J.; Zhou, X. F.; Kiraly, B.; Wood, J. D.; Alducin, D.; Myers, B. D.; Liu, X. L.; Fisher, B. L.; Santiago, U.; Guest, J. R.; et al. Synthesis of Borophenes: Anisotropic, Two-Dimensional Boron Polymorphs. *Science* **2015**, *350*, 1513−1516.
(42) Feng, B. J.; Zhang, J.; Zhong, Q.; Li, W. B.; Li, S.; Li, H.; Cheng, P.; Meng, S.; Chen, L.; Wu, K. H. Experimental Realization of Two-Dimensional Boron Sheets. *Nat. Chem.* **2016**, *8*, 563−568.
(43) Zhai, H. J.; Zhao, Y. F.; Li, W. L.; Chen, Q.; Bai, H.; Hu, H. S.; Piazza, Z. A.; Tian, W. J.; Lu, H. G.; Wu, Y. B.; et al. Observation of an All-Boron Fullerene. *Nat. Chem.* **2014**, *6*, 727−731.
(44) Chen, Q.; Li, W. L.; Zhao, Y. F.; Zhang, S. Y.; Hu, H. S.; Bai, H.; Li, H. R.; Tian, W. J.; Lu, H. G.; Zhai, H. J.; et al. Experimental and Theoretical Evidence of An Axially Chiral Borospherene. *ACS Nano* **2015**, *9*, 754−760.
(45) Chen, Q.; Zhang, S. Y.; Bai, H.; Tian, W. J.; Gao, T.; Li, H. R.; Miao, C. Q.; Mu, Y. W.; Lu, H. G.; Zhai, H. J.; et al. Cage-like B_{41}^+ and B_{42}^{2+}: New Chiral Members of the Borospherene Family. *Angew. Chem., Int. Ed.* **2015**, *54*, 8160−8164.
(46) Bean, D. E.; Fowler, P. W. Double Aromaticity in "Boron Toroids. *J. Phys. Chem. C* **2009**, *113*, 15569−15575.
(47) Jimenez-Halla, J. O. C.; Islas, R.; Heine, T.; Merino, G. B_{19}^+: An Aromatic Wankel Motor. *Angew. Chem., Int. Ed.* **2010**, *49*, 5668−5671.
(48) Zhang, J.; Sergeeva, A. P.; Sparta, M.; Alexandrova, A. N. B_{13}^+: A Photodriven Molecular Wankel Engine. *Angew. Chem., Int. Ed.* **2012**, *51*, 8512−8515.
(49) Szwacki, N. G.; Sadrzadeh, A.; Yakobson, B. I. B_{80} Fullerene: An ab Initio Prediction of Geometry, Stability, and Electronic Structure. *Phys. Rev. Lett.* **2007**, *98*, 166804.
(50) Sadrzadeh, A.; Pupysheva, O. V.; Singh, A. K.; Yakobson, B. I. The Boron Buckyball and Its Precursors: An Electronic Structure Study. *J. Phys. Chem. A* **2008**, *112*, 13679−13683.
(51) Prasad, D. L. V. K.; Jemmis, E. D. Stuffing Improves the Stability of Fullerenelike Boron Clusters. *Phys. Rev. Lett.* **2008**, *100*, 165504.
(52) Baruah, T.; Pederson, M. R.; Zope, R. R. Vibrational Stability and Electronic Structure of a B_{80} Fullerene. *Phys. Rev. B: Condens. Matter Mater. Phys.* **2008**, *78*, 045408.
(53) Nguyen, M. T.; Matus, M. H.; Ngan, V. T.; Grant, D. J.; Dixon, D. A. Thermochemistry and Electronic Structure of Small Boron and Boron Oxide Clusters and Their Anions. *J. Phys. Chem. A* **2009**, *113*, 4895−4909.
(54) De, S.; Willand, A.; Amsler, M.; Pochet, P.; Genovese, L.; Goedecker, S. Energy Landscape of Fullerene Materials: A

DOI: 10.1021/acs.jpcc.6b10958
J. Phys. Chem. C 2017, 121, 10752−10759

Comparison of Boron to Boron Nitride and Carbon. *Phys. Rev. Lett.* **2011**, *106*, 225502.
(55) Tai, T. B.; Grant, D. J.; Nguyen, M. T.; Dixon, D. A. Thermochemistry and Electronic Structure of Small Boron Clusters (B_n, n = 5−13) and Their Anions. *J. Phys. Chem. A* **2010**, *114*, 994−1007.
(56) Li, H.; Shao, N.; Shang, B.; Yuan, L.; Yang, J.; Zeng, X. C. Icosahedral B_{12}-Containing Core-Shell Structures of B_{80}. *Chem. Commun.* **2010**, *46*, 3878−3880.
(57) Zhao, J.; Wang, L.; Li, F.; Chen, Z. B_{80} and Other Medium-Sized Boron Clusters: Core-Shell Structures, Not Hollow Cages. *J. Phys. Chem. A* **2010**, *114*, 9969−9972.
(58) Wang, L.; Zhao, J.; Li, F.; Chen, Z. Boron Fullerenes with 32−56 Atoms: Irregular Cage Configurations and Electronic Properties. *Chem. Phys. Lett.* **2010**, *501*, 16−19.
(59) Li, F.; Jin, P.; Jiang, D. E.; Wang, L.; Zhang, S. B.; Zhao, J.; Chen, Z. B_{80} and $B_{101-103}$ Clusters: Remarkable Stability of the Core-Shell Structures Established by Validated Density Functionals. *J. Chem. Phys.* **2012**, *136*, 074302.
(60) Tai, T. B.; Tam, N. M.; Nguyen, M. T. Structure of Boron Clusters Revisited, B_n with n = 14−20. *Chem. Phys. Lett.* **2012**, *530*, 71−76.
(61) Lv, J.; Wang, Y. C.; Zhu, L.; Ma, Y. M. B38: An All-Boron Fullerene Analogue. *Nanoscale* **2014**, *6*, 11692−11696.
(62) Xu, S. G.; Zhao, Y. J.; Liao, J. H.; Yang, X. B. Understanding the Stable Boron Clusters: A Bond Model and First-Principles Calculations Based on High-Throughput Screening. *J. Chem. Phys.* **2015**, *142*, 214307.
(63) Zhao, J.; Huang, X.; Shi, R.; Liu, H.; Su, Y.; King, R. B. B_{28}: The Smallest All-Boron Cage From an ab Initio Global Search. *Nanoscale* **2015**, *7*, 15086−15090.
(64) Rahane, A. B.; Kumar, V. B_{84}: A Quasi-Planar Boron Cluster Stabilized with Hexagonal Holes. *Nanoscale* **2015**, *7*, 4055−4062.
(65) Romanescu, C.; Harding, D. J.; Fielicke, A.; Wang, L. S. Probing the Structures of Neutral Boron Clusters Using IR/VUV Two Color Ionization: B_{11}, B_{16}, and B_{17}. *J. Chem. Phys.* **2012**, *137*, 014317.
(66) Neumark, D. Slow Electron Velocity-Map Imaging of Negative Ions: Applications to Spectroscopy and Dynamics. *J. Phys. Chem. A* **2008**, *112*, 13287−13301.
(67) Weichman, M. L.; Devine, J. A.; Levine, D. S.; Kim, J. B.; Neumark, D. M. Isomer-Specific Vibronic Structure of the 9-, 1-, and 2-anthracenyl Radicals via Slow Photoelectron Velocity-Map Imaging. *Proc. Natl. Acad. Sci. U. S. A.* **2016**, *113*, 1698−1705.
(68) Weichman, M. L.; Devine, J. A.; Neumark, D. M. High-Resolution Photoelectron Imaging Spectroscopy of Cryogenically Cooled Fe_4O^- and Fe_5O^-. *J. Chem. Phys.* **2016**, *145*, 054302.
(69) Leon, I.; Yang, Z.; Wang, L. S. High Resolution Photoelectron Imaging of Au_2^-. *J. Chem. Phys.* **2013**, *138*, 184304.
(70) Leon, I.; Yang, Z.; Liu, H. T.; Wang, L. S. The Design and Construction of a High-Resolution Velocity-Map Imaging Apparatus for Photoelectron Spectroscopy Studies of Size-Selected Clusters. *Rev. Sci. Instrum.* **2014**, *85*, 083106.
(71) Lopez, G. V.; Czekner, J.; Jian, T.; Li, W. L.; Yang, Z.; Wang, L. S. Probing the Electronic and Vibrational Structure of $Au_2Al_2^-$ and Au_2Al_2 Using Photoelectron Spectroscopy and High Resolution Photoelectron Imaging. *J. Chem. Phys.* **2014**, *141*, 224309.
(72) Akola, J.; Manninen, M.; Hakkinen, H.; Landman, U.; Li, X.; Wang, L. S. Photoelectron Spectra of Aluminum Cluster Anions: Temperature Effects and Ab Initio Simulations. *Phys. Rev. B: Condens. Matter Mater. Phys.* **1999**, *60*, R11297−R11300.
(73) Wang, L. S.; Li, X. Temperature Effects in Anion Photoelectron Spectroscopy of Metal Clusters. In *Proc. Int. Symp. On Clusters and Nanostructure Interfaces*, Richmond, VA, Oct. 25−28, 1999; Jena, P., Khanna, S. N., Rao, B. K.; World Scientific: River Edge, NJ, 2000; pp 293−300.
(74) Huang, W.; Wang, L. S. Probing the 2D to 3D Structural Transition in Gold Cluster Anions Using Argon Tagging. *Phys. Rev. Lett.* **2009**, *102*, 153401.
(75) Dick, B. Inverting Ion Images without Abel Inversion: Maximum Entropy Reconstruction of Velocity Maps. *Phys. Chem. Chem. Phys.* **2014**, *16*, 570−580.
(76) Dribinski, V.; Ossadtchi, A.; Mandelshtam, V. A.; Reisler, H. Reconstruction of Abel-Transformable Images: The Gaussian Basis-Set Expansion Abel Transform Method. *Rev. Sci. Instrum.* **2002**, *73*, 2634−2642.
(77) Garcia, G. A.; Nahon, L.; Powis, I. Two-Dimensional Charged Particle Image Inversion Using a Polar Basis Function Expansion. *Rev. Sci. Instrum.* **2004**, *75*, 4989−4996.
(78) Cooper, J.; Zare, R. N. Angular Distribution of Photoelectrons. *J. Chem. Phys.* **1968**, *48*, 942−943.
(79) Sanov, A.; Mabbs, R. Photoelectron Imaging of Negative Ions. *Int. Rev. Phys. Chem.* **2008**, *27*, 53−85.
(80) Lee, C.; Yang, W.; Parr, R. G. Development of the Colle-Salvetti Correlation-Energy Formula into a Functional of the Electron Density. *Phys. Rev. B: Condens. Matter Mater. Phys.* **1988**, *37*, 785−789.
(81) Becke, A. D. Density-Functional Thermochemistry. III. The Role of Exact Exchange. *J. Chem. Phys.* **1993**, *98*, 5648−5652.
(82) Weigend, F.; Ahlrichs, R. Balanced Basis Sets of Split Valence, Triple Zeta Valence and Quadruple Zeta Valence Quality for H to Rn: Design and Assessment of Accuracy. *Phys. Chem. Chem. Phys.* **2005**, *7*, 3297−3305.
(83) Weigend, F. Accurate Coulomb-Fitting Basis Sets for H to Rn. *Phys. Chem. Chem. Phys.* **2006**, *8*, 1057−1065.
(84) Rappoport, D.; Furche, F. Property-optimized Gaussian basis sets for molecular response calculations. *J. Chem. Phys.* **2010**, *133*, 134105.
(85) Frisch, M. J.; Trucks, G. W.; Schlegel, H. B.; Scuseria, G. E.; Robb, M. A.; Cheeseman, J. R.; Scalmani, G.; Barone, V.; Mennucci, B.; Petersson, G. A.; et al. *Gaussian 09*, revision C.01; Gaussian, Inc.: Wallingford, CT, 2009.

DOI: 10.1021/acs.jpcc.6b10958
J. Phys. Chem. C 2017, 121, 10752−10759